IEEE Access
Multidisciplinary | Rapid Review | Open Access Journal

Received 26 July 2024, accepted 1 August 2024, date of publication 5 August 2024, date of current version 14 August 2024.

Digital Object Identifier 10.1109/ACCESS.2024.3438791

RESEARCH ARTICLE

Pole Placement Technique Optimized Gains by Adaptive Tabu Search for Instability Mitigation of AC–DC Power System Feeding a Controlled Buck Converter

JAKKRIT PAKDEETO[1], ALISA THANOMMUANG[2], KONGPOL AREERAK[2], (Member, IEEE), AND KONGPAN AREERAK[2], (Member, IEEE)

[1]Department of Teacher Training in Electrical Engineering, Faculty of Technical Education, King Mongkut's University of Technology North Bangkok (KMUTNB), Bangkok 10800, Thailand
[2]School of Electrical Engineering, Institute of Engineering, Suranaree University of Technology, Nakhon Ratchasima 30000, Thailand

Corresponding author: Kongpan Areerak (kongpan@sut.ac.th)

This work was supported by the Suranaree University of Technology (SUT), Thailand.

ABSTRACT Power converters with tightly regulations are known to behave as constant power loads, which can degrade the stability of the system. Therefore, system stabilization using the pole placement technique, in which the feedback gains are optimized by the adaptive Tabu search (ATS) algorithm, is introduced in this paper. Additionally, the averaging model of the power converter is used to compute the system response and eigenvalues during the searching process. Therefore, better output responses can be provided by the resulting feedback gains than those designed by the conventional method. Moreover, the application of the pole placement technique designed by the ATS algorithm confirms the operation of the system under stable conditions. The effectiveness of the proposed design technique is verified using simulation and experimental results.

INDEX TERMS Instability mitigation, pole placement technique, optimal controller design, adaptive Tabu search.

I. INTRODUCTION

With the current advancement of power electronic technologies [1], the use of power converters in numerous engineering applications, such as aerospace and submarine industries, grid connections, and appliances, has been increasing. These technologies are continuously developed to address the needs of various power ranges of alternating current (AC) and direct current (DC) electricity. Most of these converters might be controlled to serve the desired purposes. However, the controlled power converters behave as negative impedances, called ''constant power loads (CPLs)'' [2], [3], [4], that can degrade the stability of the system, in which unstable operation might occur under the rated power. The unstable operation of the system over an unstable point is dangerous for system components and users. Hence, the stability analysis is required to clarify the difficulty encountered at the unstable point. From the literature reviews [5], [6], [7], [8], [9], numerous methods to analyze system stability, in which two major groups can be categorized as linear and nonlinear stability analysis. Stability analysis via the time-invariant model utilizes both groups [10], [11], [12]. For the nonlinear stability analysis, predicting the unstable point using the nonlinear time-invariant model is more complicated than using the small-signal theorem. Thus, the linear stability analysis is used in this paper to avoid the unstable point of the power system. However, the stability analysis can only predict the unstable point, in which the considered system cannot be employed until the rated power [10], [13]. Therefore, mitigation methods for the unstable point of the power system using the pole placement technique will be presented in this paper [14], [15] in which it can be applied in almost all

The associate editor coordinating the review of this manuscript and approving it for publication was Feiqi Deng.

applications feeding the CPLs. When the pole placement technique is added to the system, it can prevent system instability.

Literature reviews [16], [17], [18] reveal passive and active damping to mitigate the unstable point. Passive damping is easy to design and simple to implement. However, the insertion of passive components into the system will increase power losses. In addition, the costs of system modification and passive devices in passive damping might be more expensive than in active damping. Hence, active damping will be presented in this paper to mitigate the system instability for the AC–DC power system feeding a controlled buck converter. The active technique can be modified for the feeder and load sides or even added to the auxiliary circuit [10]. However, the considered system lacks switches at the feeder side, and the additional auxiliary circuit can increase the costs of the system. Fortunately, the controlled buck converter is on the load side of the considered system and can be modified by the active damping in the controller. Thus, the stabilization of active damping through the considered system at the load side is presented in this paper. Several approaches [18], [19], [20] to the active damping technique have been presented to eliminate the effect of CPLs. One of these approaches is the pole placement method [14], [21], which can be employed to design the dominant poles of the system. These poles can be fixed at the desired location using the feedback pole placement loop gains, facilitating the stable operation of the system when the dominant poles are located on the left-hand side (LHS) of the s-plane [22]. The limitation of the pole placement method lies in the complexity of designing all state feedback gains. The participation factor is also used in this paper to reduce the number of state feedbacks and eliminate some state variables that are not significant to the instability. Afterward, the remaining state variables are crucial and will be multiplied by the designed pole placement gains. The SimPowerSystem® block set on the MATLAB program can be used to confirm the stable operation via the simulation result. Despite the stability of the system using the proposed technique, the performance of the system response should still be considered. The artificial intelligence (AI) techniques reported in [23], [24], [25], and [26] are used in numerous engineering applications to achieve optimal system response. The adaptive Tabu search (ATS), which has been reported on the searching performance to achieve the global solution [27], [28], will be utilized for the pole placement gain design to realize the optimal response. The proposed design is expected to yield superior results to the conventional design. The main advantages of the proposed optimal design are as follows:

1) The system instability can be mitigated by employing the pole placement technique. However, the important state variables are also evaluated by the participation factor to reduce the number of state feedbacks.

2) The ATS is applied to design the feedback gains to provide optimal output voltage response of the controlled buck converter, which has not been reported in previous studies.

3) Other AI techniques can also be applied to provide optimal feedback gains by following the concept presented in this paper.

Simulation and experimental results are used to verify the effectiveness of the proposed mitigation method.

The results show that the system can be stabilized using the proposed mitigation technique until the rated power is realized. Moreover, the pole placement parameters obtained from the ATS can provide superior performance compared with those from the conventional design.

This paper is organized into six sections. Section I introduces the background problems. Section II provides the considered system with a constant power load, which is affected by the system stability. In addition, this section provides the details of stability analysis via the eigenvalue theorem. Section III presents the pole placement technique used to mitigate the unstable operation and the participation factor used to reduce the number of state variables. Section IV addresses the design method of the pole placement parameters using conventional methods and the proposed ATS algorithm. Section V shows the experimental results, and Section VI presents the conclusions.

II. CONSIDERED SYSTEM WITH THE CPL EFFECT

Fig. 1 (gray area) depicts the AC–DC power system feeding a controlled buck converter. This system comprises three parts: the first part is the source side, which has a balanced three-phase voltage source and a transmission line feeding the power into the six-pulse diode rectifier, including the DC link filters. This rectifier is used to convert AC to DC. For the second part, the load of the considered system is a regulated buck converter used for stepdown voltage from the output of the diode rectifier. The last part is the cascade PI controller used for the output voltage regulation of a buck converter. For the cascade PI controller, the outer loop is used for voltage regulation, while the current through the inductor is controlled using an inner loop. The buck converter behaves as a constant power load when its output voltage is controlled, and the CPL can substantially degrade the stability of the system [29]. Hence, the stability analysis is crucial to provide information when the system is unstable and avoid the unstable point.

The mathematical model is required for the stability analysis. The literature reviews [11], [30], [31], [32] revealed several techniques to derive the time-invariant mathematical model, which is suitable for stability analysis. The DQ method [11] is highly popular for the three-phase power system, while the DC/DC converter can be derived using the GSSA method [30]. The time-invariant model can be obtained for the considered system using a combination of these methods. Furthermore, the basic circuit theory involving Kirchhoff's voltage law and Kirchhoff's current law is applied. Therefore, the time- invariant model of the considered AC–DC power system feeding a controlled buck converter can be expressed in (1), as shown at the bottom of the next page.

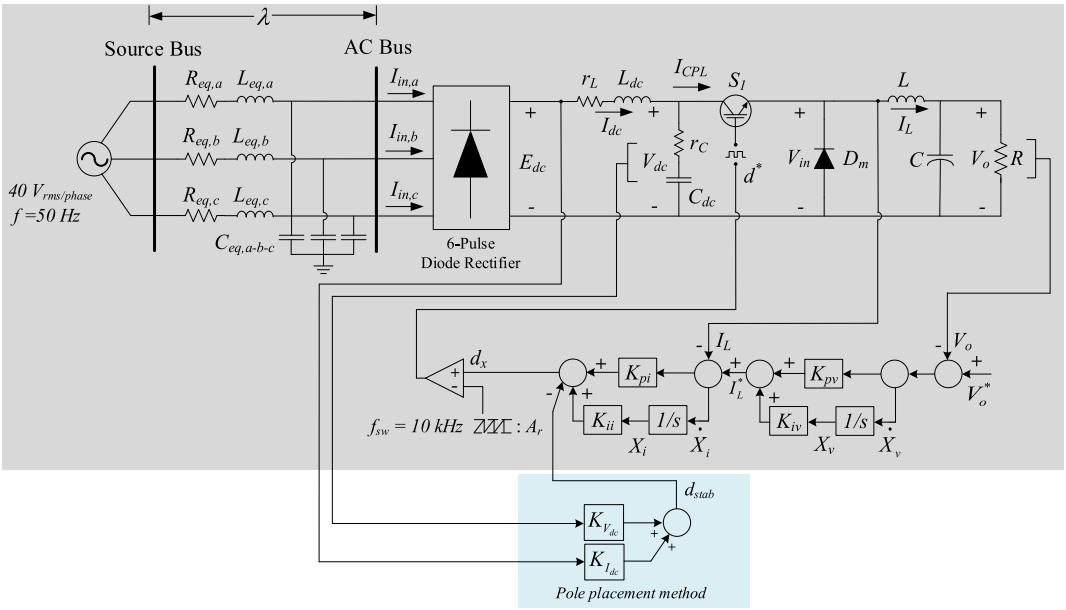

FIGURE 1. Considered system with stabilization by pole placement technique.

Extensive details to derive the proposed model are presented in [20]. Equation (1) presents a time-invariant model of the considered AC–DC power system feeding a controlled buck converter without using the pole placement technique to mitigate the unstable operation. However, this nonlinear model has a state variable multiplication. The eigenvalue theorem for the stability analysis cannot be applied to the model of (1). Thus, the first-order term of Taylor's series expansion [33] is used to linearize the model of (1) to obtain the linearized model, as shown in (2).

$$\begin{cases} \delta\dot{\mathbf{x}} = \mathbf{A}(\mathbf{x_0}, \mathbf{u_0})\delta\mathbf{x} + \mathbf{B}(\mathbf{x_0}, \mathbf{u_0})\delta\mathbf{u} \\ \delta\mathbf{y} = \mathbf{C}(\mathbf{x_0}, \mathbf{u_0})\delta\mathbf{x} + \mathbf{D}(\mathbf{x_0}, \mathbf{u_0})\delta\mathbf{u} \end{cases} \tag{2}$$

where the state variables are $\delta\,\mathbf{x} = [\delta I_{sd}\ \delta I_{sq}\ \delta V_{bus,d}\ \delta V_{bus,q}\ \delta I_{dc}\ \delta V_{dc}\ \delta I_L\ \delta V_o\ \delta X_v\ \delta X_i]^T$, the input variables are $\delta\mathbf{u} = [\delta V_m\ \delta V_o^*]^T$, and the output variables are $\delta\mathbf{y} = [\delta I_{dc}\ \delta V_{dc}\ \delta I_L$

$$\begin{cases} \dot{I}_{sd} = -\dfrac{R_{eq}}{L_{eq}} I_{sd} + \omega I_{sq} - \dfrac{1}{L_{eq}} V_{bus,d} + \dfrac{1}{L_{eq}}\sqrt{\dfrac{3}{2}} V_m \cos(\lambda) \\ \dot{I}_{sq} = -\omega I_{sd} - \dfrac{R_{eq}}{L_{eq}} I_{sq} - \dfrac{1}{L_{eq}} V_{bus,q} + \dfrac{1}{L_{eq}}\sqrt{\dfrac{3}{2}} V_m \sin(\lambda) \\ \dot{V}_{bus,d} = \dfrac{1}{C_{eq}} I_{sd} + \omega V_{bus,q} - \sqrt{\dfrac{3}{2}}\dfrac{2\sqrt{3}}{\pi C_{eq}} I_{dc} \\ \dot{V}_{bus,q} = \dfrac{1}{C_{eq}} I_{sq} - \omega V_{bus,d} \\ \dot{I}_{dc} = \sqrt{\dfrac{3}{2}}\dfrac{2\sqrt{3}}{\pi L_{eq}} V_{bus,d} - \dfrac{(r_\mu + r_L + r_C)}{L_{dc}} I_{dc} - \dfrac{1}{L_{dc}} V_{dc} \\ + \dfrac{r_C K_{pv} K_{pi}}{A_r L_{dc}} V_o^* I_L - \dfrac{r_C K_{pv} K_{pi}}{A_r L_{dc}} V_o I_L + \dfrac{r_C K_{pi} K_{iv}}{A_r L_{dc}} X_v I_L + \dfrac{r_C K_{pi}}{A_r L_{dc}} I_L^2 + \dfrac{r_C K_{ii}}{A_r L_{dc}} X_i I_L \\ \dot{V}_{dc} = \dfrac{1}{C_{dc}} I_{dc} - \dfrac{K_{pv} K_{pi}}{C_{dc}} V_o^* I_L + \dfrac{K_{pv} K_{pi}}{C_{dc}} V_o I_L - \dfrac{K_{pi} K_{iv}}{C_{dc}} X_v I_L + \dfrac{K_{pi}}{C_{dc}} I_L^2 - \dfrac{K_{ii}}{C_{dc}} X_i I_L \\ \dot{I}_L = \dfrac{K_{pv} K_{pi}}{L} V_o^* V_{dc} - \dfrac{K_{pv} K_{pi}}{L} V_o V_{dc} + \dfrac{K_{pi} K_{iv}}{L} X_v V_{dc} - \dfrac{K_{pi}}{L} I_L V_{dc} + \dfrac{K_{ii}}{L} X_i V_{dc} - \dfrac{V_o}{L} \\ \dot{V}_o = \dfrac{1}{C} I_L - \dfrac{1}{RC} V_o \\ \dot{X}_v = V_o^* - V_o \\ \dot{X}_i = -I_L - K_{pv} V_o + K_{pv} V_o^* + K_{iv} X_v \end{cases} \tag{1}$$

$\delta V_o]^T$. The details of matrices A, B, C, and D can be found in the Appendix.

After the linearized model is obtained, the stability analysis using the eigenvalue theorem can be calculated using (3).

$$\det[\lambda \mathbf{I} - \mathbf{A}] = 0 \tag{3}$$

The system remains in a stable operation if $real\lambda_i < 0$ while i is the pole amount of the system. For the considered system, the value of power (P_{CPL}) will change when the command output voltage (V_o^*) of the controlled buck converter is varied. The eigenvalues for varying P_{CPL} can be illustrated in Fig. 2, and the system parameters are shown in Table 1.

Fig. 2 shows the variation of V_o^* from 46 V to 50, 54, and 58 V, corresponding to 211.6, 250, 291.6, and 336.4 W, respectively. The zoom area in Fig. 2 shows the movement of the dominant poles. When the V_o^* is equal to 54 V (P_{CPL} = 291.6 W), the dominant poles are located in the right-hand side (RHS) of the s-plane. Therefore, the system has an unstable operation at this power level based on the eigenvalue's theorem [9]. Fig. 3 depicts the simulation results using the SimPowerSystem® block set on the MATLAB program to verify the results from the stability analysis.

As shown in Fig. 3, the V_o will be increased. After t = 3 s, the V_o is equal to 54 V (291.6 W), and the unstable

TABLE 1. System parameters.

Parameters	Values	Descriptions
V_s	40 $V_{rms/phase}$	Three-phase voltage source
ω	2π×50 rad/s	Three-phase source frequency
R_{eq}	0.079 Ω	Resistance of transmission line equivalent circuit
L_{eq}	0.1005 mH	Inductance of transmission line equivalent circuit
C_{eq}	2 nF	Capacitance of transmission line equivalent circuit
r_L	0.2756 Ω	Inner resistance of inductor in the filter circuit
L_{dc}	39.0002 mH	Inductance of the filter circuit
r_C	0.5312 Ω	Inner resistance of the capacitor in the filter circuit
C_{dc}	1300 µF	Capacitance of the filter circuit
$L(\Delta I_L \leq 0.2\ \mathrm{A})$	30 mH	Inductance of buck converter
$C(\Delta V_C \leq 2.8\ \mathrm{mV})$	1000 µF	Capacitance of buck converter
R	10 Ω	Resistive load of buck converter
A_r	10	Peak amplitude of carrier signal
K_{pv}	0.0257	Proportional gain of voltage loop
K_{iv}	3.9478	Integral gain of voltage loop
K_{pi}	2.8205	Proportional gain of current loop
K_{ii}	2531.7	Integral gain of current loop

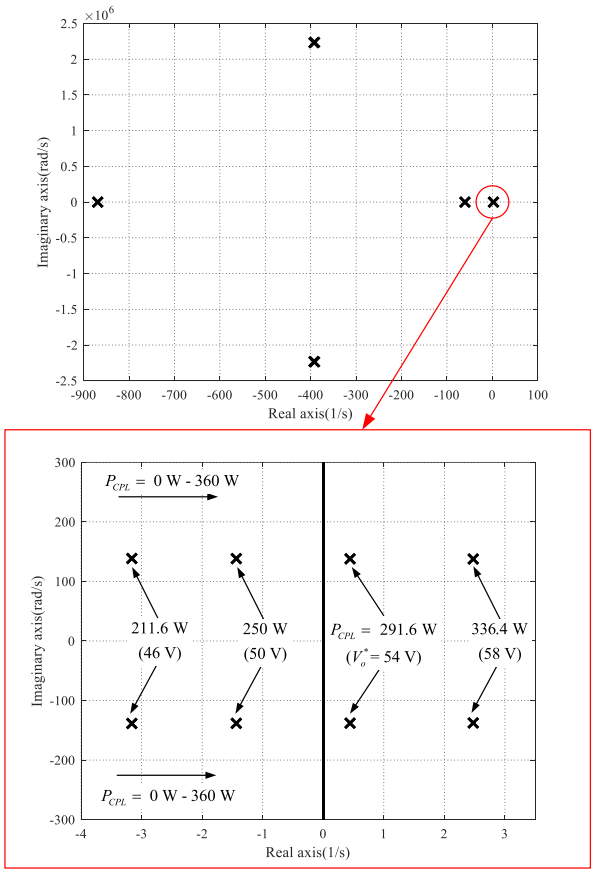

FIGURE 2. Eigenvalues for stability analysis.

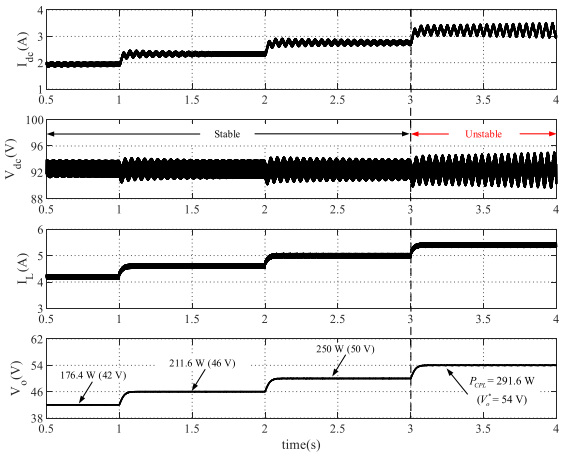

FIGURE 3. Simulation result for stability analysis.

operation will occur in the considered system. The responses after t = 3 s will be inconsistent with the steady-state value, thereby damaging the system components. Thus, the unstable operation may occur before the rated power (300 W) can be realized. However, the unstable operation not only affects the performance of the system but may also be risky for their clients. In this case, the stability analysis can only predict the unstable point and fails to stabilize the operation of the system until the rated power is realized. Therefore, instability

mitigation is necessary to maintain the stable operation of the considered system until a rated power of 300 W is realized. Section III describes the stabilization using the proposed pole placement method.

III. INSTABILITY MITIGATION USING POLE PLACEMENT TECHNIQUE

The pole placement technique is applied in this paper to mitigate the instability of the system. The principle of the pole placement approach [14], [15] lies in all state variable feedbacks through the gains of the inner **K** vector, as shown in Fig. 4.

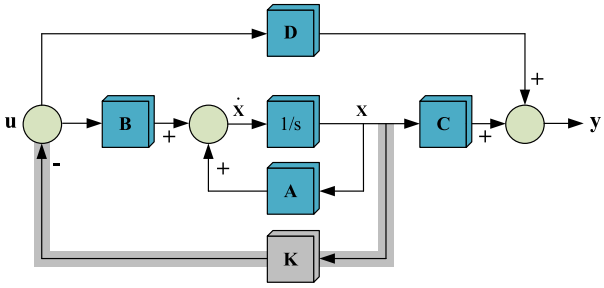

FIGURE 4. Pole placement principle.

The state space model without the **K** feedback can generally be expressed in (4). As shown in Fig. 4 (gray line), if the pole placement is focused, then all state variables (**x**) will be multiplied with the **K** vector to obtain the feedback signal as the new input variable of the model, as shown in (5).

$$\begin{cases} \dot{\mathbf{x}} = \mathbf{A}(\mathbf{x},\mathbf{u})\mathbf{x} + \mathbf{B}(\mathbf{x},\mathbf{u})\mathbf{u} \\ \mathbf{y} = \mathbf{C}(\mathbf{x},\mathbf{u})\mathbf{x} + \mathbf{D}(\mathbf{x},\mathbf{u})\mathbf{u} \end{cases} \tag{4}$$

$$\mathbf{u} = -\mathbf{K}\mathbf{x} \tag{5}$$

The state space model, including the pole placement feedback, can be shown in (6) by substituting (5) in (4). This model is the **K** vector, that is, the unknown values depending on the number of state variables. Conventionally, the **K** vectors could be designed by the characteristic equation set equal to the polynomial equation of the desired poles, as shown in (7) [34].

$$\begin{cases} \dot{\mathbf{x}} = (\mathbf{A}(\mathbf{x},\mathbf{u}) - \mathbf{B}(\mathbf{x},\mathbf{u})\mathbf{K})\mathbf{x} \\ \mathbf{y} = (\mathbf{C}(\mathbf{x},\mathbf{u}) - \mathbf{D}(\mathbf{x},\mathbf{u})\mathbf{K})\mathbf{x} \end{cases} \tag{6}$$

$$\det(s\mathbf{I} - (\mathbf{A}(\mathbf{x},\mathbf{u}) - \mathbf{B}(\mathbf{x},\mathbf{u})\mathbf{K})) = \prod_{i=1}^{n}(s - p_i) \tag{7}$$

where $\prod_{i=1}^{n}(s - p_i)$ are the sum of the multiplication obtained from the desired dominant pole (p_i) locations, and n is the maximum order of the polynomial equation in which it is equal to the amount of state variables.

The mentioned pole placement principle can be applied to several available systems to provide a similar state variable model to the model in (1). However, the proposed model demonstrates some variables (not all states) that can be measured in the practical testing rig as follows: I_{dc}, V_{dc}, I_L, and V_o. These signals can be obtained via the current and voltage sensors for feeding into the microcontroller board. Hence, the pole placement technique applied to the considered system for instability mitigation can only be designed from four unknown variables in the **K** vector. The participation factor is utilized to reduce the amount of state variable feedback. The participation factor is used to identify the substantial variables affecting the system stability [20]. Three steps for analyzing the participation factor are presented as follows: the first step involves the process of eigenvalue matrix calculation from (3). In addition, the right eigenvector (**v**) and the left eigenvector (**w**) matrices can be calculated by (8) and (9), respectively. Both eigenvector matrix values can be found in the appendix. For the second step, the dominant mode of the eigenvalue matrix is defined as follows: if any real values (σ_i) of the eigenvalue ($\lambda_i = \sigma_i \pm j\omega_i$) have $|\sigma_i| < \varepsilon$ (near the imaginary axis) or $\sigma_i > 0$ (located at RHS) at the unstable operation, then this mode is considered dominant. The third step is the participation matrix calculation by (10) for identifying the maximum values at the dominant mode. The rows of the participation matrix can provide the significant state variables that have the most effect on the system stability. Table 2 shows the result of the participation factor process.

$$\mathbf{A}\mathbf{v} = \lambda\mathbf{v} \tag{8}$$

$$\mathbf{w}^T\mathbf{A} = \lambda\mathbf{w}^T \tag{9}$$

$$\text{Participation Matrix} = |\mathbf{w} \cdot \mathbf{v}| \tag{10}$$

TABLE 2. Participation matrix for considered system without mitigation case.

	Col. I	Col. II	...	Col.VII	Col.VIII	Col. IX	Col. X
I_{sd}	0.4959	0.4959	⋯	0.0024	0.0024	0.0000	0.0000
I_{sq}	0.0013	0.0013	⋯	0.0000	0.0000	0.0000	0.0000
	⋮	⋮		⋮	⋮	⋮	⋮
I_{dc}	0.0033	0.0033	⋯	0.5119	0.5119	0.0087	0.0087
V_{dc}	0.0000	0.0000	⋯	0.5050	0.5050	0.0009	0.0009
	⋮	⋮		⋮	⋮	⋮	⋮
X_i	0.0000	0.0000	...	0.0103	0.0103	0.1045	0.1045

As shown in Table 2, I_{dc} and V_{dc} are the most important variables for the dominant mode. The parameters related to the important variables are L_{dc} and C_{dc}. If the current through L_{dc} and voltage across C_{dc} can be adjusted using the $K_{I_{dc}}$ and $K_{V_{dc}}$ values, respectively, of the inner **K** vector, then the dominant poles of the considered AC–DC power system will be also relocated. Therefore, the pole placement technique used in this paper to mitigate the unstable operation will use only I_{dc} and V_{dc} can be multiplied with the designed $K_{I_{dc}}$ and $K_{V_{dc}}$ feedback values, respectively, into the controller. The advantage of the participation factor process lies in its

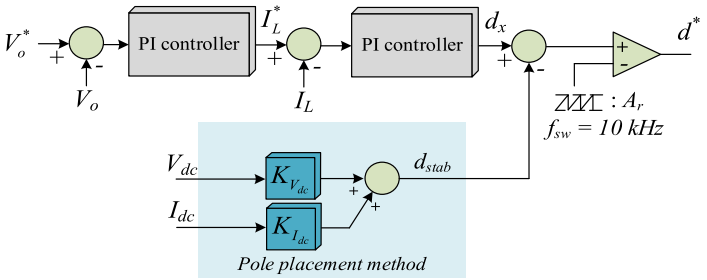

FIGURE 5. PI controller of buck converter modified with the pole placement gains.

reduction of the irrelevant state variables. In addition, this factor is used to evaluate the prominent values for decreasing the complicated calculation.

As shown in Fig. 1 (blue area), the pole placement feedback gains can be added into the conventional cascade PI controller to modify the control structure of the considered system at the load side. Fig. 5 illustrates the zoom area from Fig. 1. The $K_{I_{dc}}$ and $K_{V_{dc}}$ will be multiplied with the I_{dc} and V_{dc}, respectively, to calculate the compensated control signal d_{stab}. Fig. 5 reveals the dstab, which can be calculated using (11).

$$d_{stab} = K_{I_{dc}} I_{dc} + K_{V_{dc}} V_{dc} \tag{11}$$

The d_{stab} will be subtracted from the conventional output control signal of the cascade PI controller (d_x), as shown in Fig. 5. Thus, the d^*, in which the time-invariant model of the considered system, including the pole placement technique, can be calculated in (12), as shown at the bottom of the next page, to mitigate the unstable operation as shown in (13), as shown at the bottom of the next page.

After obtaining the dynamic model of the considered power system with the pole placement technique, the proposed technique variables ($K_{I_{dc}}$ and $K_{V_{dc}}$) are not only found in the rows of I_{dc} and V_{dc} but are also in I_L, as shown in (13). These variables will be used for instability mitigation to demonstrate their independence. In the first step before the $K_{I_{dc}}$ and $K_{V_{dc}}$ designed by the ATS algorithm, these gains can be designed to demonstrate the dominant pole relocation using trial and error. The dominant poles at the V_o^* equal to 54 V (291.6 W) can relocate from the RHS using $K_{I_{dc}} = 1.0$ and $K_{V_{dc}} = -0.025$, as depicted in Fig. 6. This condition is the instability mitigation because the dominant poles can be moved back to the LHS of the s-plane. The simulation results are illustrated in Fig. 7 to confirm the mentioned mitigation concept. These results are categorized into two scenarios: stabilization using $K_{I_{dc}} = 1.0$ and $K_{V_{dc}} = -0.025$ and nonstabilization ($K_{I_{dc}} = 0$ and $K_{V_{dc}} = 0$) cases.

As shown in the simulation results in Fig. 7, in the case of nonstabilization, the system will be unstable after t = 2 s while the V_o^* was increased from 50 V (250 W) to 54 V (291.6 W). Otherwise, the considered system can still maintain a stable operation at the same condition by setting $K_{I_{dc}} = 1.0$ and $K_{V_{dc}} = -0.025$. The results confirm that the proposed concept for the stabilization using the pole placement is successful. Section IV describes the design methods of these gains of pole placement technique using the ATS method.

IV. POLE PLACEMENT DESIGN

As described in the principle in Section III, the pole placement technique is used to stabilize the considered system. This section will present the design methods of $K_{I_{dc}}$ and $K_{V_{dc}}$, in which two methods are presented in this paper. The first method is the sufficiently small value evaluation called "conventional pole placement design."

The eigenvalue theorem is used to inspect the dominant poles based on the mathematical model. The ATS approach is another method used to provide the optimal pole placement parameters. The details of the two methods are presented as follows:

A. CONVENTIONAL POLE PLACEMENT DESIGN

The evaluation of $K_{I_{dc}}$ and $K_{V_{dc}}$ using the conventional pole placement design has a sufficiently small value to mitigate the unstable operation.

The system poles of the considered system at $V_o^* = 58$V(336.4 W) are evaluated when the gains $K_{I_{dc}}$ and $K_{V_{dc}}$ are varied, as shown in Fig. 8. As shown in Table 2, the $K_{I_{dc}}$ is slightly more dominant than $K_{V_{dc}}$. Hence, $K_{I_{dc}}$ is initially varied, while $K_{V_{dc}}$ will be fixed equal to 0, as shown in Fig. 8(a). The dominant poles will be moved to LHS when $K_{I_{dc}}$ is increased. Thus, the sufficiently small value [34] is chosen, in which the $K_{I_{dc}}$ will be equal to one. In Fig. 8(b), $K_{I_{dc}}$ is fixed equal to 0, while the $K_{V_{dc}}$ will also be varied. It differs from the $K_{I_{dc}}$ case in which the $K_{V_{dc}}$ must be decreased to mitigate the unstable operation. Fig. 8(b) shows that the dominant poles will be located in the LHS when $K_{V_{dc}} = -1.5$. This method will provide the $K_{I_{dc}} = 1$ and $K_{V_{dc}} = -1.5$ to stabilize the considered system; thus, selecting these parameters due to the randomness of $K_{I_{dc}}$ and $K_{V_{dc}}$ is complicated. Hence, this paper will introduce another way to design these gains using the AI technique, as described below.

B. OPTIMAL POLE PLACEMENT DESIGN

The pole placement gains will be designed in this section using the ATS algorithm to provide the superior performance to those designed using the conventional method. The block

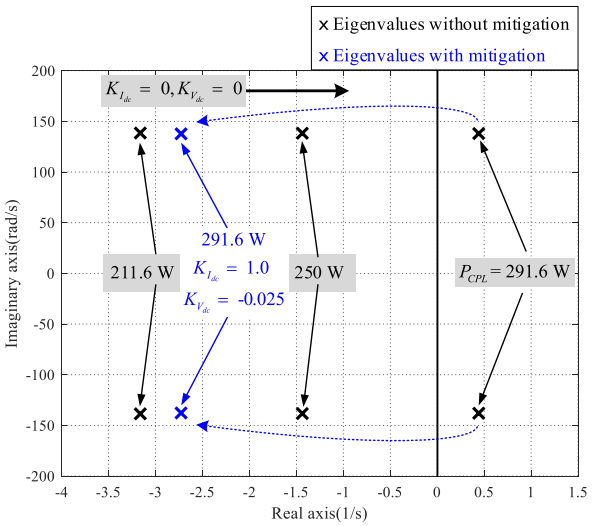

FIGURE 6. Trajectory dominant poles involving pole placement gains.

diagram of the optimal pole placement design is illustrated in Fig. 9, which presents comprehensive details of the ATS, as shown in [20] and [27]

As shown in Fig. 9, the V_o response can be calculated from the linearized model. This response will be used to calculate the cost value (W) depending on rise time (T_r), settling time (T_s), and overshoot percentage ($P.O.$). The ATS technique will tune the $K_{I_{dc}}$ and $K_{V_{dc}}$ values within the defined boundary to calculate the W. The ATS will search the pole placement gains until the minimum W is achieved. The following presents details of the searching process to provide the optimal pole placement parameters:

Step 1: Set the ATS parameters such as radius (R) equal to 20, and the maximum iteration ($Round_{\max}$) is equal to 100. The boundaries of $K_{I_{dc}}$ and $K_{V_{dc}}$ are set equal to (0.0–20.0) and (−3.0–0.0), respectively, in this paper. Fig. 8 shows the estimated values from the conventional pole placement design. However, the $K_{V_{dc}}$ is set to the lower boundary as −3.0 because the dominant poles will be backward to the RHS after $K_{V_{dc}} < -3.0$, as depicted in Fig. 8(b).

Step 2: Randomly set the initial solution (S_0) in the searching boundary area, as shown in Fig. 10. In this step, the S_0 can be called "local solution" and matched to *best_neighbor*. Thus, the $K_{I_{dc}}$ and $K_{V_{dc}}$ are random in the defined boundaries and assumed to be the *best_neighbor* in the next step.

Step 3: Randomly choose N (neighborhood) as the new solutions around S_0 within the boundary of radius R. Define $S_1(r)$ as a solution set with N number of solutions, as shown in Fig. 11. Therefore, the $K_{I_{dc}}$ and $K_{V_{dc}}$ are random in the defined boundaries according to the R radius as the solution set. In this paper, N was set equal to 40; thus, $K_{I_{dc}}$ and $K_{V_{dc}}$ have solutions that are equal to 40 sets.

$$\begin{cases} d^* = \dfrac{1}{A_r}\left(d_x - d_{stab}\right) \\ d^* = \dfrac{1}{A_r}\left(K_{pv}K_{pi}V_o^* - K_{pv}K_{pi}V_o + K_{pi}K_{iv}X_v - K_{pi}I_L + K_{ii}X_i\right) \end{cases} \tag{12}$$

$$\begin{cases} \dot{I}_{sd} = -\dfrac{R_{eq}}{L_{eq}}I_{sd} + \omega I_{sq} - \dfrac{1}{L_{eq}}V_{bus,d} + \dfrac{1}{L_{eq}}\sqrt{\dfrac{3}{2}}V_m\cos(\lambda) \\ \dot{I}_{sq} = -\omega I_{sd} - \dfrac{R_{eq}}{L_{eq}}I_{sq} - \dfrac{1}{L_{eq}}V_{bus,q} + \dfrac{1}{L_{eq}}\sqrt{\dfrac{3}{2}}V_m\sin(\lambda) \\ \dot{V}_{bus,d} = \dfrac{1}{C_{eq}}I_{sd} + \omega V_{bus,q} - \sqrt{\dfrac{3}{2}}\dfrac{2\sqrt{3}}{\pi C_{eq}}I_{dc} \\ \dot{V}_{bus,q} = \dfrac{1}{C_{eq}}I_{sq} - \omega V_{bus,d} \\ \dot{I}_{dc} = \sqrt{\dfrac{3}{2}}\dfrac{2\sqrt{3}}{\pi L_{eq}}V_{bus,d} - \dfrac{(r_\mu + r_L + r_C)}{L_{dc}}I_{dc} - \dfrac{1}{L_{dc}}V_{dc} + \dfrac{r_C K_{pv}K_{pi}}{A_r L_{dc}}V_o^* I_L - \dfrac{r_C K_{pv}K_{pi}}{A_r L_{dc}}V_o I_L + \dfrac{r_C K_{pi}K_{iv}}{A_r L_{dc}}X_v I_L - \dfrac{r_C K_{pi}}{A_r L_{dc}}I_L^2 \\ + \dfrac{r_C K_{ii}}{A_r L_{dc}}X_i I_L - \dfrac{r_C K_{I_{dc}}}{A_r L_{dc}}I_{dc}I_L - \dfrac{r_C K_{V_{dc}}}{A_r L_{dc}}V_{dc}I_L \\ \dot{V}_{dc} = \dfrac{1}{C_{dc}}I_{dc} - \dfrac{K_{pv}K_{pi}}{A_r C_{dc}}V_o^* I_L + \dfrac{K_{pv}K_{pi}}{A_r C_{dc}}V_o I_L - \dfrac{K_{pi}K_{iv}}{A_r C_{dc}}X_v I_L + \dfrac{K_{pi}}{A_r C_{dc}}I_L^2 - \dfrac{K_{ii}}{A_r C_{dc}}X_i I_L + \dfrac{K_{I_{dc}}}{A_r C_{dc}}I_{dc}I_L + \dfrac{K_{V_{dc}}}{A_r C_{dc}}V_{dc}I_L \\ \dot{I}_L = \dfrac{K_{pv}K_{pi}}{A_r L}V_o^* V_{dc} - \dfrac{K_{pv}K_{pi}}{A_r L}V_o V_{dc} + \dfrac{K_{pi}K_{iv}}{A_r L}X_v V_{dc} - \dfrac{K_{pi}}{A_r L}I_L V_{dc} + \dfrac{K_{ii}}{A_r L}X_i V_{dc} - \dfrac{K_{I_{dc}}}{A_r L}I_{dc}V_{dc} - \dfrac{K_{V_{dc}}}{A_r L}V_{dc}^2 - \dfrac{V_o}{L} \\ \dot{V}_o = \dfrac{1}{C}I_L - \dfrac{1}{RC}V_o \\ \dot{X}_v = V_o^* - V_o \\ \dot{X}_i = -I_L - K_{pv}V_o + K_{pv}V_o^* + K_{iv}X_v \end{cases} \tag{13}$$

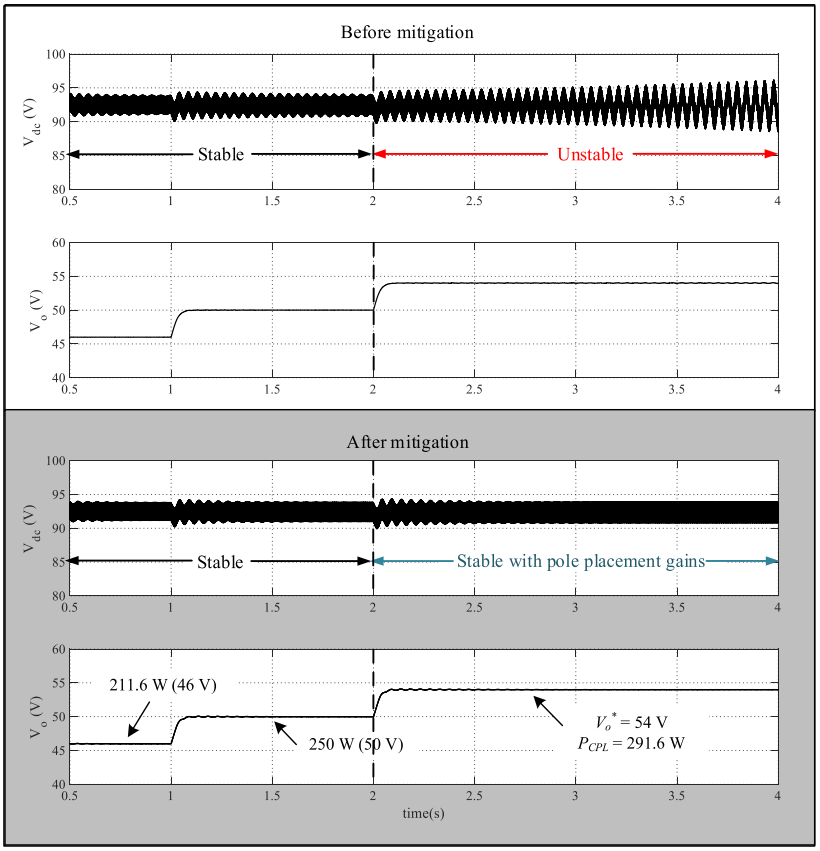

FIGURE 7. Simulation results for instability mitigation.

Step 4: Evaluate the members of $S_1(r)$ using the objective function. The S_1 will be set as the best solution of $S_1(r)$. The best solution is assigned as the *best_neighbor*1, as shown in Fig. 11. This step is used to evaluate the entire $S_1(r)$ members, providing the best solution with members that are random values of $K_{I_{dc}}$ and $K_{V_{dc}}$.

As shown in Fig. 8, the V_o obtained from the mathematical model depends on system parameters and pole placement loop gains ($K_{I_{dc}}$ and $K_{V_{dc}}$). If these gains are varied while other parameters are fixed, then dominant poles will be moved and the V_o response will be changed. Therefore, evaluating the entire $S_1(r)$ members is important to achieve the stable operation in each iteration by adjusting $K_{I_{dc}}$ and $K_{V_{dc}}$ values. These values are not only used to mitigate the unstable operation but are also affected by system performance. $K_{I_{dc}}$ and $K_{V_{dc}}$ are obtained from $S_1(r)$ members to evaluate the system performance, and the V_o will be used to calculate the $T_{r,ATS}$, $T_{s,ATS}$, and $P.O._{ATS}$. In addition, the $T_{r,CONV}$, $T_{s,CONV}$, and $P.O._{CONV}$ values can be obtained from conventional pole placement design ($K_{I_{dc}} = 1$ and $K_{V_{dc}} = -1.5$), as expressed in (14).

$$W = \alpha\left(\frac{T_{r,ATS}}{T_{r,CONV}}\right) + \beta\left(\frac{T_{s,ATS}}{T_{s,CONV}}\right) + \gamma\left(\frac{P.O._{ATS}}{P.O._{CONV}}\right) \tag{14}$$

where α, β, and γ are the concerned weight coefficients.

The weight coefficients will be defined in this paper as equal because $T_{r,ATS}$, $T_{s,ATS}$, and $P.O._{ATS}$ are equally significant, and the summation of these values will be 100%. For stability analysis, the eigenvalues are also calculated via the linearized model for each solution during the searching process. If the $Re\,(\lambda_i) < 0$ is unsatisfied (unstable operation), then the W is set to the large value ($W \approx 10000$) as the penalty for the minimization problem. Therefore, the optimal pole placement parameters can provide the best system response, including the achievement of stable operation in this step.

Step 5: If *best_neighbor*1 has a better value than *best_neighbor*, then *best_neighbor* will be set equal to *best_neighbor*1 in the Tabu list and $S_0 =$ *best_neighbor*, as depicted in Figs. 12 and 13, respectively. However, if the *best_neighbor*1 remains unidentified, then the searching process returns to step 3 until the best solution is achieved under the $Round_{\max}$. Thus, the best value in every iteration will be identified and used as the new center point of searching in the next iteration. Fig. 14 illustrates the next process when *best_neighbor*1 is obtained.

Step 6: This step was added to the conventional Tabu search [35], in which the backtracking mechanism and the adaptive radius exist. For the backtracking mechanism, the best solution from the Tabu list will be selected and then assigned as the new initial solution for the next iteration, as shown in Fig. 15.

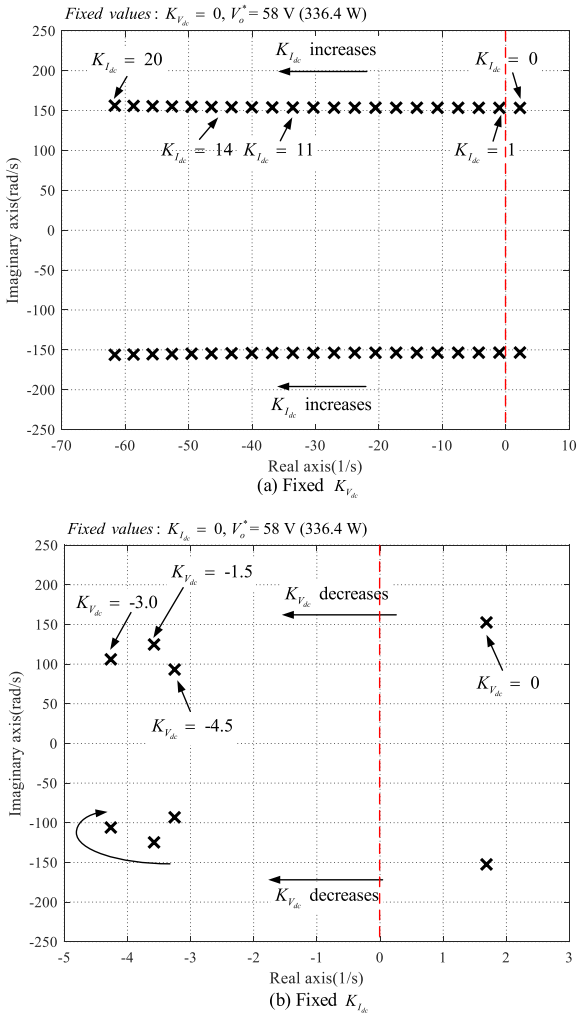

FIGURE 8. Conventional pole placement design.

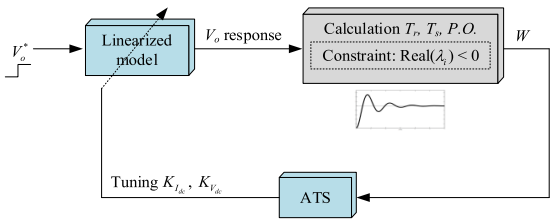

FIGURE 9. Block diagram of the pole placement design.

The maximum iteration of the repeated best solution is set equal to 10 for this research. The backtracking mechanism will return to the best solution in the Tabu list after the best solution repeats more than 10 times. This mechanism can change in a new direction, which is a different route for discovering the global solution. As for the adaptive radius, the searching boundary will be decreased, as shown in Fig. 16. The equation for decreasing radius can be calculated in (15), in which the decreasing factor ($D.F.$) will be equal to 1.5, rapidly determining the global solution. The proposed concept can be applied with other AI algorithms, but the ATS is still used in this paper because this algorithm can escape the local solution until the global solution is achieved [27]. The specifications of the personal computer which was used for the ATS are as follows: Intel(R) Core(TM) i7-10700 CPU @ 2.90GHz, RAM 16 GB, and 64-bit operating system on Windows 10. This computer consumes the computational cost,

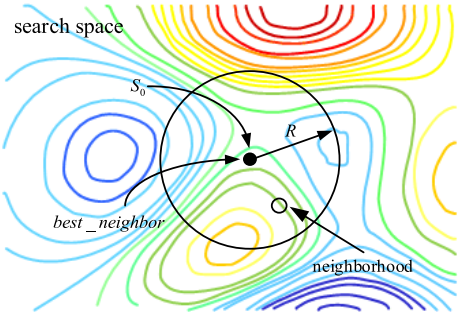

FIGURE 10. Random S_0 in searching the boundary.

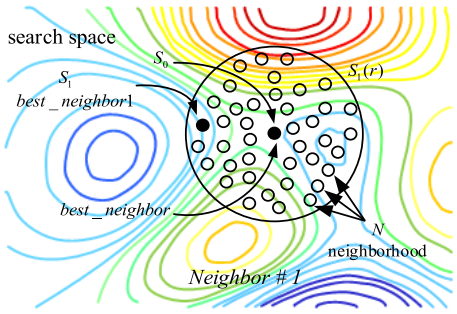

FIGURE 11. Random neighborhood around S_0 as a solution set $S_1(r)$.

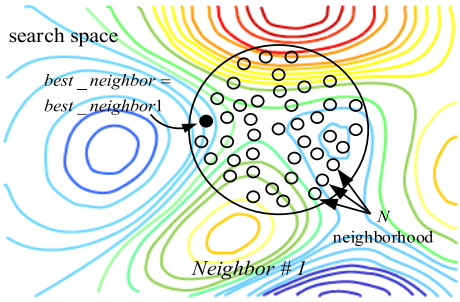

FIGURE 12. Define the new *best_neighbor*.

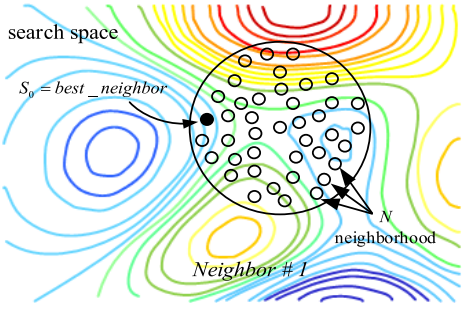

FIGURE 13. Define the new S_0 = *best_neighbor*.

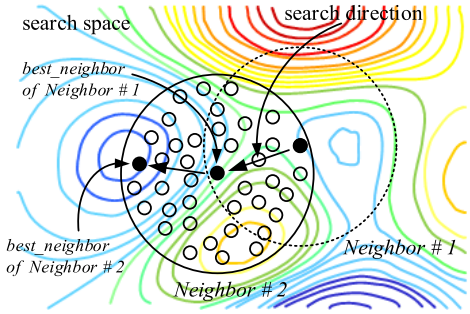

FIGURE 14. Searching process in the next iteration.

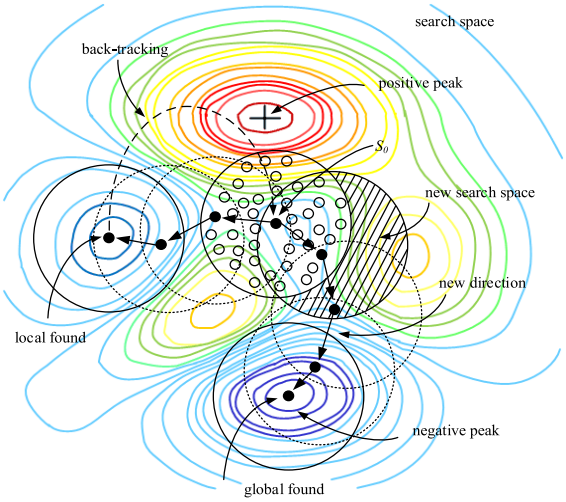

FIGURE 15. New direction obtained from the backtracking mechanism.

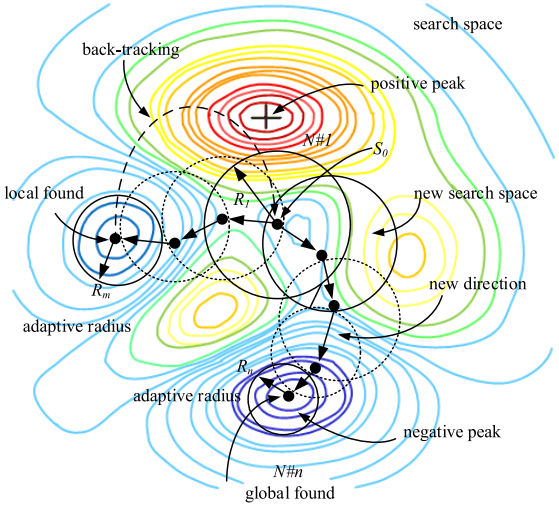

FIGURE 16. Adaptive radius of ATS.

running time, and inference time for the proposed optimal controller design using the ATS as shown in Table 3 where these values can be counted from the MATLAB program. The definitions of these values can be found in [36].

$$radius_{new} = \frac{radius_{old}}{D.F.} \tag{15}$$

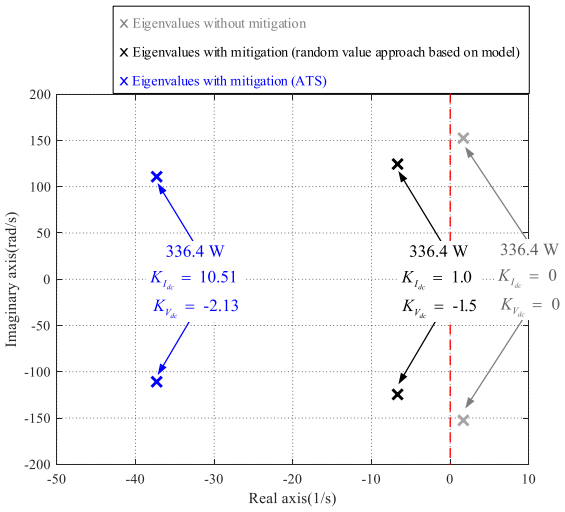

FIGURE 17. Eigenvalue evaluation of the considered system at V_o^* equal to 58 V (336.4 W).

TABLE 3. Pole placement parameters at V_o^* equal to 58 V (336.4 W).

Parameters	Designed method	
	Conventional Design	ATS Design
$K_{I_{dc}}$	1.0	10.51
$K_{V_{dc}}$	−1.5	−2.13
Cost value (W)	1.0	0.6474
Iteration (rounds)	-	100
Computational cost (s)	-	2.23
Running time (s)	-	6816.82
Inference time (s)	-	112.97

Table 3 shows the resulting gains after the ATS is completed in 100 iterations which are the stop time criteria for ATS processes. Compared with the conventional design, the optimized pole placement parameters can provide the best. Hence, the pole placement parameters obtained from the ATS algorithm can be used to mitigate the unstable operation with a superior response compared with the conventional design.

The dominant poles will be depicted in Fig. 17 to confirm the pole placement parameters from Table 3, in which V_o^* equal to 58 V (336.4 W) is the concerned operating point.

As shown in Fig. 17, the dominant poles can be moved to the LHS of the s-plane using both pole placement designs. Therefore, the considered system can be stabilized with the proposed mitigation technique. However, the system responses should also be considered because the superior output response should be achieved as expected from the ATS design technique. Fig. 18 illustrates the simulation results using the SimPowerSystem® block set in MATLAB.

As shown in Fig. 18, after $t = 1.5$ s, the system will be an unstable operation in the case before mitigation

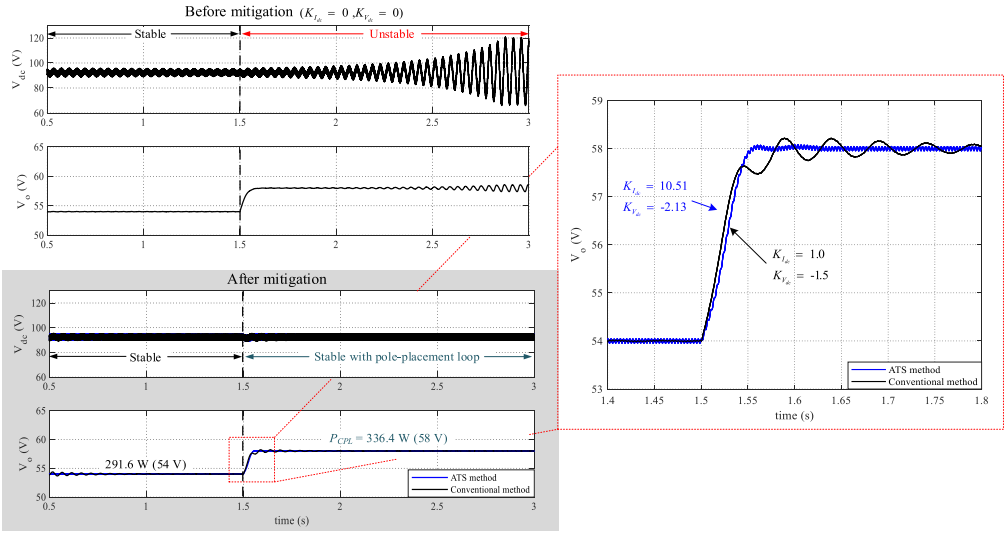

FIGURE 18. Simulation results at V_o^* equal to 58 V (336.4 W).

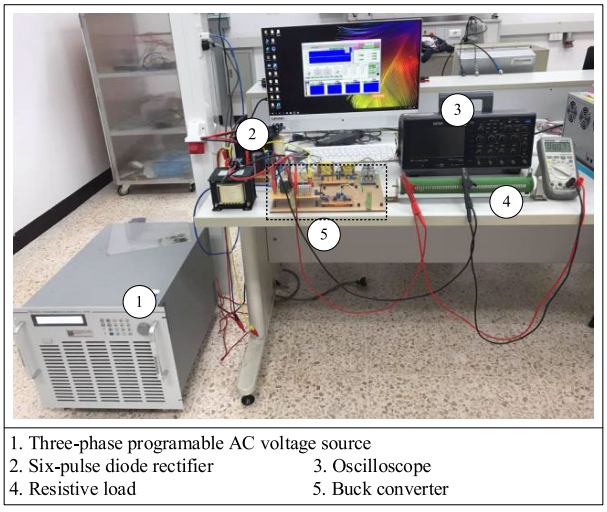

1. Three-phase programable AC voltage source
2. Six-pulse diode rectifier
3. Oscilloscope
4. Resistive load
5. Buck converter

FIGURE 19. Experimental rig of considered system.

($K_{I_{dc}} = 0$ and $K_{V_{dc}} = 0$). However, the system responses will be stabilized using the proposed technique after mitigation (gray area). The zoom area of Fig. 18 is displayed to compare the response performance, in which the black and blue lines are the responses from conventional and ATS methods, respectively. The pole placement parameters from the ATS design can provide better performance compared with those from the conventional design. In addition to the simulation comparison, this paper will also introduce the experimental results in Section V.

V. EXPERIMENTAL RESULTS

Fig. 19 illustrates the testing rig used in this research. This rig comprises a three-phase programable AC voltage source for feeding the power into the six-pulse diode rectifier circuit. The output voltage and current of rectifier

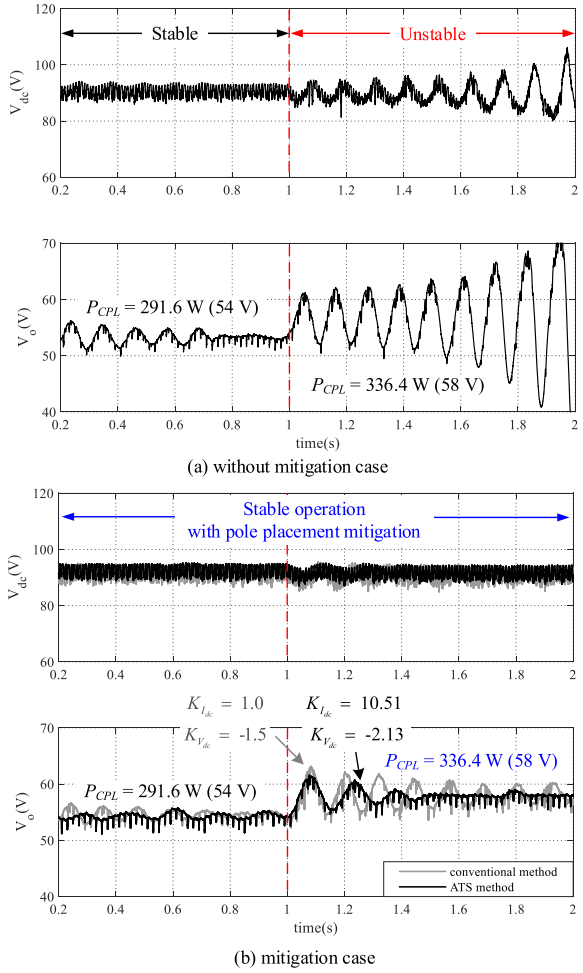

FIGURE 20. Experimental results operated with pole placement mitigation.

are filtered by an LC filter. The DC output voltage of the buck converter is regulated using the cascade PI controllers

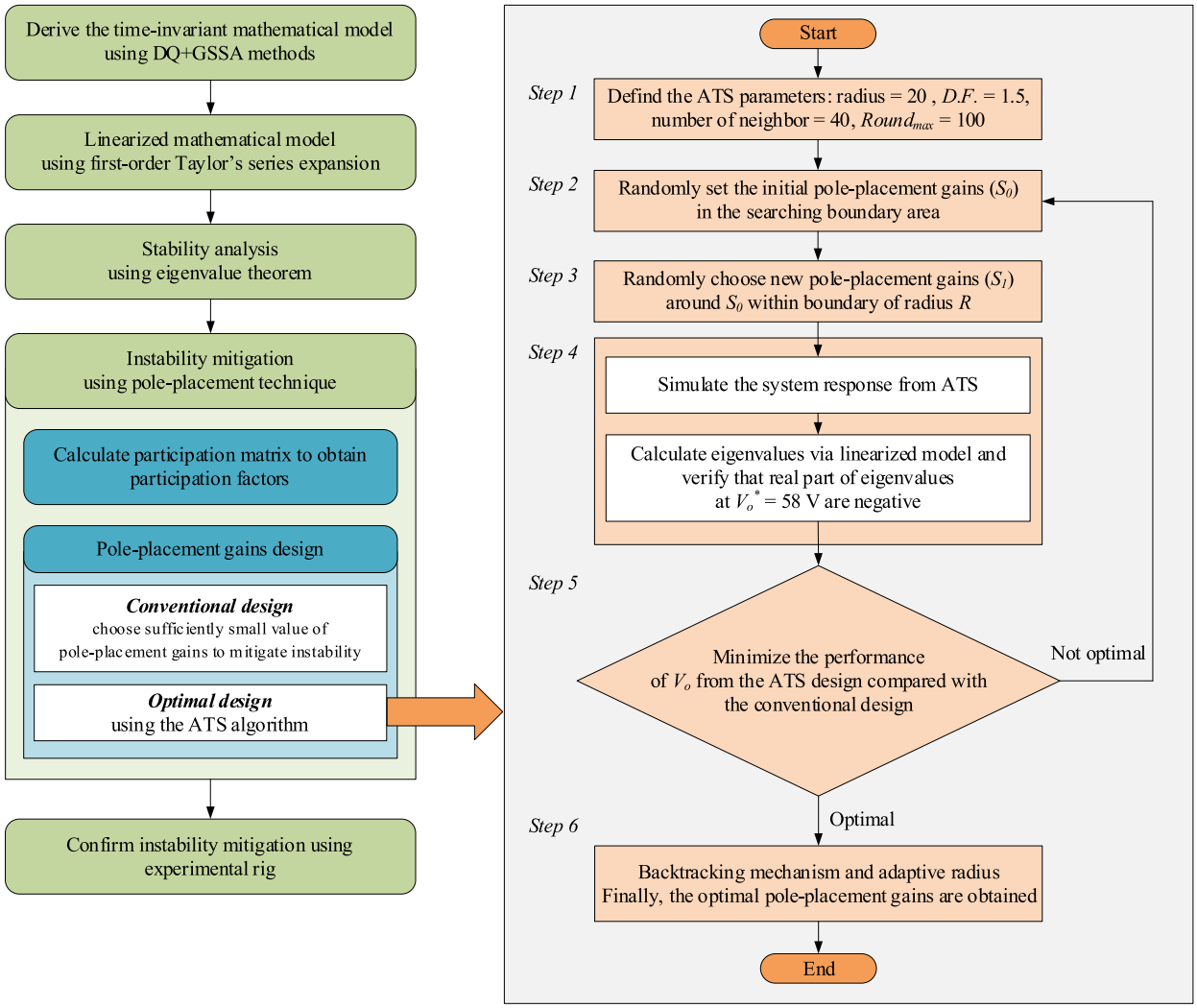

FIGURE 21. Work flow diagram of the proposed method.

implemented by the Arduino Mega 2560 as a microcontroller. For the mitigation process, the voltage and current sensors are required to measure the voltage and current signals from the filter circuit. These signals are sent to the microcontroller and used for calculating the compensated control signal by the pole-placement method. In addition, the oscilloscope is used to collect the responses from the experimental rig.

As shown in Fig. 17, the dominant poles are located in the RHS in the case without mitigation ($K_{I_{dc}} = 0$ and $K_{V_{dc}} = 0$) after the eigenvalues are analyzed. However, these poles can be moved to LHS when $K_{I_{dc}}$ and $K_{V_{dc}}$ are used. The results from the testing rig can be illustrated in Fig. 20 to confirm this analysis using the experiment.

Fig. 20(a) shows the unstable operation of the system underrated power in the case without mitigation. Conversely, the system is stabilized beyond the rated power (300 W) when the $K_{I_{dc}}$ and $K_{V_{dc}}$ are used in the pole placement loop, as shown in Fig. 20(b). The two design methods proposed in this paper can be used for instability mitigation. However, in terms of performance, the parameters of the pole placement technique obtained from the ATS design can provide better performance compared with the

TABLE 4. Performance comparison at V_o^* 58 V (336.4 W).

Design method	Overshoot percentage	Settling time (sec.)	Rise time (sec.)
Simulation			
Conventional method	0.0937	0.1273	0.0499
ATS method	0.0733	0.1035	0.0499
Experiment			
Conventional method	8.6450	0.5852	0.0491
ATS method	5.0962	0.2568	0.0491

conventional design. Fig. 20(b) shows the improved performance of the system. The performance comparison focuses on the values of overshoot percentage, rise time and settling time as addressed in Table 4. The simulation and experimental results show that the mitigation parameters designed from the ATS can provide the superior performance compared with those designed from the conventional method.

VI. CONCLUSION

This paper presents the pole placement technique to mitigate the unstable operation of the AC–DC power system feeding a controlled buck converter. The work flow diagram of the entire process and the procedure of the ATS algorithm for designing the pole-placement gains can be summarized as shown in Fig. 21. From the stability analysis via the eigenvalue theorem, the system instability occurred before the rated power. The proposed technique can be used to stabilize the system until the rated power is realized. In addition, the principle of pole placement technique is introduced, and the participation factor is applied to reduce the number of state feedbacks. The remaining variables are significantly dominant to system stability. In addition, two design methods for the pole placement parameters are presented in this paper. However, the proposed technique still requires the voltage and current sensors installed into to the DC bus. These sensors are used for measuring the essential data for the microcontroller board. The simulation results using the SimPowerSystem® in MATLAB show that the parameters obtained from the ATS design can yield superior performance compared with the conventional design. Moreover, the experimental results are presented to ensure that the proposed technique can be used to mitigate the unstable operation in accordance with the analysis and simulation results.

$$\mathbf{A}(\mathbf{x_0},\mathbf{u_0}) = \begin{bmatrix} -\frac{R_{eq}}{L_{eq}} & \omega & -\frac{1}{L_{eq}} & 0 & 0 & 0 & 0 & 0 & 0 & 0 \\ -\omega & -\frac{R_{eq}}{L_{eq}} & 0 & -\frac{1}{L_{eq}} & 0 & 0 & 0 & 0 & 0 & 0 \\ \frac{1}{C_{eq}} & 0 & 0 & \omega & -\frac{S_d}{C_{eq}} & 0 & 0 & 0 & 0 & 0 \\ 0 & \frac{1}{C_{eq}} & -\omega & 0 & 0 & 0 & 0 & 0 & 0 & 0 \\ 0 & 0 & \frac{S_d}{L_{dc}} & 0 & -\frac{(r_\mu+r_L+r_C)}{L_{dc}} & -\frac{1}{L_{dc}} & a(5,7) & -\frac{r_C K_{pv} K_{pi} I_{L,0}}{A_r L_{dc}} & \frac{r_C K_{pi} K_{iv} I_{L,0}}{A_r L_{dc}} & \frac{r_C K_{ii} I_{L,0}}{A_r L_{dc}} \\ 0 & 0 & 0 & 0 & \frac{1}{C_{dc}} & 0 & a(6,7) & \frac{K_{pv} K_{pi} I_{L,0}}{A_r C_{dc}} & -\frac{K_{pi} K_{iv} I_{L,0}}{A_r C_{dc}} & -\frac{K_{ii} I_{L,0}}{A_r C_{dc}} \\ 0 & 0 & 0 & 0 & 0 & a(7,6) & -\frac{K_{pi} V_{dc,0}}{A_r L} & -\frac{K_{pv} K_{pi} V_{dc,0}}{A_r L} - \frac{1}{L} & \frac{K_{pi} K_{iv} V_{dc,0}}{A_r L} & \frac{K_{ii} V_{dc,0}}{A_r L} \\ 0 & 0 & 0 & 0 & 0 & 0 & \frac{1}{C} & -\frac{1}{RC} & 0 & 0 \\ 0 & 0 & 0 & 0 & 0 & 0 & 0 & -1 & 0 & 0 \\ 0 & 0 & 0 & 0 & 0 & 0 & -1 & -K_{pv} & K_{iv} & 0 \end{bmatrix}_{10\times 10}$$

$$a(5,7) = \frac{r_C K_{pv} K_{pi} V_o^*}{A_r L_{dc}} - \frac{r_C K_{pv} K_{pi} V_o}{A_r L_{dc}} + \frac{r_C K_{pi} K_{iv} X_v}{A_r L_{dc}} - \frac{2 r_C K_{pi} I_L}{A_r L_{dc}} + \frac{r_C K_{ii} X_i}{A_r L_{dc}}$$

$$a(6,7) = -\frac{K_{pv} K_{pi} V_o^*}{A_r C_{dc}} + \frac{K_{pv} K_{pi} V_o}{A_r C_{dc}} - \frac{K_{pi} K_{iv} X_v}{A_r C_{dc}} + \frac{2 K_{pi} I_L}{A_r C_{dc}} - \frac{K_{ii} X_i}{A_r C_{dc}}$$

$$a(7,6) = \frac{K_{pv} K_{pi} V_o^*}{A_r L} - \frac{K_{pv} K_{pi} V_o}{A_r L} + \frac{K_{pi} K_{iv} X_v}{A_r L} - \frac{K_{pi} I_L}{A_r L} + \frac{K_{ii} X_i}{A_r L}$$

$$\mathbf{B}(\mathbf{x_0},\mathbf{u_0}) = \begin{bmatrix} \sqrt{\frac{3}{2}}\frac{\cos(\lambda_0)}{L_{eq}} & 0 \\ \sqrt{\frac{3}{2}}\frac{\sin(\lambda_0)}{L_{eq}} & 0 \\ 0 & 0 \\ 0 & 0 \\ 0 & \frac{r_C K_{pv} K_{pi} I_{L,0}}{L_{dc}} \\ 0 & -\frac{K_{pv} K_{pi} I_{L,0}}{C_{dc}} \\ 0 & \frac{K_{pv} K_{pi} V_{dc,0}}{L} \\ 0 & 0 \\ 0 & 1 \\ 0 & K_{pv} \end{bmatrix}_{10\times 2}$$

$$\mathbf{C}(\mathbf{x_0},\mathbf{u_0}) = \begin{bmatrix} 0 & 0 & 0 & 0 & 0 & 1 & 0 & 0 & 0 & 0 \\ 0 & 0 & 0 & 0 & 0 & 0 & 0 & 1 & 0 & 0 \end{bmatrix}_{2\times 10}$$

$$\mathbf{D}(\mathbf{x_0},\mathbf{u_0}) = \begin{bmatrix} 0 & 0 \\ 0 & 0 \end{bmatrix}_{2\times 2}$$

TABLE 5. Right eigenvector matrix.

	Col. I	Col. II	…	Col.VII	Col.VIII	Col. IX	Col. X
Row. I.	-7.8×10^{-7} $+4.4\times10^{-3}$j	-7.8×10^{-7} -4.4×10^{-3}j	…	-4.3×10^{-2} $+2.3\times10^{-1}$j	-4.3×10^{-2} -2.3×10^{-1}j	8.6×10^{-2} $+1.4\times10^{-2}$j	8.6×10^{-2} -1.4×10^{-2}j
Row. II.	-2.7×10^{-4} -1.4×10^{-7}j	-2.7×10^{-4} $+1.4\times10^{-7}$j	…	6.2×10^{-9} -1.1×10^{-8}j	6.2×10^{-9} $+1.1\times10^{-8}$j	-3.6×10^{-9} -7.1×10^{-10}j	-3.6×10^{-9} $+7.1\times10^{-10}$j
…	⋮	⋮		⋮	⋮	⋮	⋮
Row. V.	-2.6×10^{-9} -1.5×10^{-5}j	-2.6×10^{-9} $+1.5\times10^{-5}$j	…	-3.2×10^{-2} $+1.7\times10^{-1}$j	-3.2×10^{-2} -1.7×10^{-1}j	6.4×10^{-2} $+1.0\times10^{-2}$j	6.4×10^{-2} -1.0×10^{-2}j
Row. VI	-5.3×10^{-9} $+1.8\times10^{-12}$j	-5.3×10^{-9} -1.8×10^{-12}j	…	9.5×10^{-1}	9.5×10^{-1}	1.3×10^{-1} -1.2×10^{-2}j	1.3×10^{-1} $+1.2\times10^{-2}$j
…	⋮	⋮		⋮	⋮	⋮	⋮
Row. X.	-4.2×10^{-20} -3.0×10^{-24}j	-4.2×10^{-20} $+3.0\times10^{-24}$j	…	-2.3×10^{-5} $+4.0\times10^{-6}$j	-2.3×10^{-5} -4.0×10^{-6}j	4.0×10^{-5} -4.2×10^{-7}j	4.0×10^{-5} $+4.2\times10^{-7}$j

TABLE 6. Left eigenvector matrix.

	Col. I	Col. II	…	Col.VII	Col.VIII	Col. IX	Col. X
Row. I.	-9.1×10^{-5} $+1.1\times10^{2}$j	-9.1×10^{-5} -1.1×10^{2}j	…	2.1×10^{-5} $+1.0\times10^{-2}$j	2.1×10^{-5} -1.0×10^{-2}j	-1.6×10^{-4} $+4.4\times10^{-4}$j	-1.6×10^{-4} -4.4×10^{-4}j
Row. II.	-6.7 -2.3×10^{-3}j	-6.7 $+2.3\times10^{-3}$j	…	1.8×10^{-10} $+5.0\times10^{-10}$j	1.8×10^{-10} -5.0×10^{-10}j	-6.0×10^{-12} $+1.9\times10^{-11}$j	-6.0×10^{-12} -1.9×10^{-11}j
…	⋮	⋮		⋮	⋮	⋮	⋮
Row. V.	5.2×10^{-2} -1.5×10^{2}j	5.2×10^{-2} $+1.5\times10^{2}$j	…	6.0×10^{-3} +2.9j	6.0×10^{-3} -2.9j	-4.6×10^{-2} $+1.3\times10^{-1}$j	-4.6×10^{-2} -1.3×10^{-1}j
Row. VI	-1.7×10^{-3} -9.1×10^{-7}j	-1.7×10^{-3} $+9.1\times10^{-7}$j	…	5.2×10^{-1} $+9.5\times10^{-2}$j	5.2×10^{-1} -9.5×10^{-2}j	4.1×10^{-3} -5.2×10^{-3}j	4.1×10^{-3} $+5.2\times10^{-3}$j
…	⋮	⋮		⋮	⋮	⋮	⋮
Row. X.	1.3 $+8.6\times10^{-4}$j	1.3 -8.6×10^{-4}j	…	-3.1×10^{-2} -7.2×10^{1}j	-3.1×10^{-2} $+7.2\times10^{1}$j	5.5×10^{2} -2.6×10^{3}j	5.5×10^{2} $+2.6\times10^{3}$j

APPENDIX

The details of Jacobian's matrix in (2) are presented as follows, $\mathbf{A}(\mathbf{x_0}, \mathbf{u_0})$, $\mathbf{B}(\mathbf{x_0}, \mathbf{u_0})$, $\mathbf{C}(\mathbf{x_0}, \mathbf{u_0})$ and $\mathbf{D}(\mathbf{x_0}, \mathbf{u_0})$ as shown at the bottom of the previous page.

The details of right eigenvector ($\mathbf{v}$) and left eigenvector ($\mathbf{w}$) in (8) and (9) are presented as follows, see Tables 5 and 6.

REFERENCES

[1] R. B. Gonzatti, Y. Li, M. Amirabadi, B. Lehman, and F. Z. Peng, "An overview of converter topologies and their derivations and interrelationships," *IEEE J. Emerg. Sel. Topics Power Electron.*, vol. 10, no. 6, pp. 6417–6429, Dec. 2022.

[2] C. Rivetta, G. A. Williamson, and A. Emadi, "Constant power loads and negative impedance instability in sea and undersea vehicles: Statement of the problem and comprehensive large-signal solution," in *Proc. IEEE Electric Ship Technol. Symp.*, 2005, pp. 313–320.

[3] A. Emadi, A. Khaligh, C. H. Rivetta, and G. A. Williamson, "Constant power loads and negative impedance instability in automotive systems: Definition, modeling, stability, and control of power electronic converters and motor drives," *IEEE Trans. Veh. Technol.*, vol. 55, no. 4, pp. 1112–1125, Jul. 2006.

[4] S. Singh, A. R. Gautam, and D. Fulwani, "Constant power loads and their effects in DC distributed power systems: A review," *Renew. Sustain. Energy Rev.*, vol. 72, pp. 407–421, May 2017.

[5] K.-N. Areerak, S. V. Bozhko, G. M. Asher, and D. W. P. Thomas, "Stability analysis and modelling of AC-DC system with mixed load using DQ-transformation method," in *Proc. IEEE Int. Symp. Ind. Electron.*, Jun. 2008, pp. 19–24.

[6] A. Griffo, J. Wang, and D. Howe, "Large signal stability analysis of DC power systems with constant power loads," in *Proc. IEEE Vehicle Power Propuls. Conf.*, 2008, pp. 1–6.

[7] Y. Huangfu, S. Pang, B. Nahid-Mobarakeh, L. Guo, A. K. Rathore, and F. Gao, "Stability analysis and active stabilization of on-board DC power converter system with input filter," *IEEE Trans. Ind. Electron.*, vol. 65, no. 1, pp. 790–799, Jan. 2018.

[8] M. A. Pai and P. W. Sauer, "Stability analysis of power systems by Lyapunov's direct method," *IEEE Control Syst. Mag.*, vol. SM-9, no. 1, pp. 23–27, Jan. 1989.

[9] A. Riccobono and E. Santi, "Comprehensive review of stability criteria for DC distribution systems," in *Proc. IEEE Energy Convers. Congr. Exposit. (ECCE)*, Sep. 2012, pp. 3917–3925.

[10] K. Areerak, T. Sopapirm, S. Bozhko, C. I. Hill, A. Suyapan, and K. Areerak, "Adaptive stabilization of uncontrolled rectifier based AC–DC power systems feeding constant power loads," *IEEE Trans. Power Electron.*, vol. 33, no. 10, pp. 8927–8935, Oct. 2018.

[11] K.-N. Areerak, S. V. Bozhko, G. M. Asher, and D. W. P. Thomas, "DQ-transformation approach for modelling and stability analysis of AC-DC power system with controlled PWM rectifier and constant power loads," in *Proc. 13th Int. Power Electron. Motion Control Conf.*, Sep. 2008, pp. 2049–2054.

[12] Y. Hong, Z. Shuai, H. Cheng, C. Tu, Y. Li, and Z. J. Shen, "Stability analysis of low-frequency oscillation in train-network system using RLC circuit model," *IEEE Trans. Transport. Electrific.*, vol. 5, no. 2, pp. 502–514, Jun. 2019.

[13] J. Pakdeeto, K. Areerak, S. Bozhko, and K. Areerak, "Stabilization of DC MicroGrid systems using the loop-cancellation technique," *IEEE J. Emerg. Sel. Topics Power Electron.*, vol. 9, no. 3, pp. 2652–2663, Jun. 2021.

[14] S. Kim and S. S. Williamson, "Negative impedance instability compensation in buck converter using state space pole placement control," in *Proc. 25th IEEE Can. Conf. Electr. Comput. Eng. (CCECE)*, Apr. 2012, pp. 1–5.

[15] S. Kim and S. S. Williamson, "Negative impedance instability compensation in more electric aircraft DC power systems using state space pole placement control," in *Proc. IEEE Vehicle Power Propuls. Conf.*, Sep. 2011, pp. 1–6.

[16] E. Hossain, R. Perez, A. Nasiri, and S. Padmanaban, "A comprehensive review on constant power loads compensation techniques," *IEEE Access*, vol. 6, pp. 33285–33305, 2018.
[17] M. Cespedes, L. Xing, and J. Sun, "Constant-power load system stabilization by passive damping," *IEEE Trans. Power Electron.*, vol. 26, no. 7, pp. 1832–1836, Jul. 2011.
[18] M. A. Hassan, C.-L. Su, J. Pou, G. Sulligoi, D. Almakhles, D. Bosich, and J. M. Guerrero, "DC shipboard microgrids with constant power loads: A review of advanced nonlinear control strategies and stabilization techniques," *IEEE Trans. Smart Grid*, vol. 13, no. 5, pp. 3422–3438, Sep. 2022.
[19] A. M. Rahimi, G. A. Williamson, and A. Emadi, "Loop-cancellation technique: A novel nonlinear feedback to overcome the destabilizing effect of constant-power loads," *IEEE Trans. Veh. Technol.*, vol. 59, no. 2, pp. 650–661, Feb. 2010.
[20] R. Phosung, K. Areerak, T. Sopapirm, and K. Areerak, "Design and optimization of instability mitigation for AC–DC feeder systems with constant power loads using artificial intelligence techniques," *IEEE Trans. Power Electron.*, vol. 37, no. 5, pp. 5385–5397, May 2022.
[21] M. U. Iftikhar, E. Godoy, P. Lefranc, D. Sadarnac, and C. Karimi, "A control strategy to stabilize PWM DC–DC converters with input filters using state-feedback and pole-placement," in *Proc. IEEE 30th Int. Telecommun. Energy Conf. (INTELEC)*, Sep. 2008, pp. 1–5.
[22] M. Wu and D. D. Lu, "A novel stabilization method of LC input filter with constant power loads without load performance compromise in DC microgrids," *IEEE Trans. Ind. Electron.*, vol. 62, no. 7, pp. 4552–4562, Jul. 2015.
[23] M. Nutakki and S. Mandava, "Review on optimization techniques and role of artificial intelligence in home energy management systems," *Eng. Appl. Artif. Intell.*, vol. 119, Mar. 2023, Art. no. 105721.
[24] P. Khluabwannarat, "Parallel flower pollination algorithm and its application to fractional-order PID controller design optimization for BLDC motor speed control system," *Przeglad Elektrotechniczny*, vol. 1, no. 11, pp. 80–85, Nov. 2020.
[25] J. Nowaková and M. Pokorný, "Intelligent controller design by the artificial intelligence methods," *Sensors*, vol. 20, no. 16, p. 4454, Aug. 2020.
[26] A. Swarnkar and A. Swarnkar, "Artificial intelligence based optimization techniques: A review," in *Intelligent Computing Techniques for Smart Energy Systems*. Singapore: Springer, 2020, pp. 95–103.
[27] D. Puangdownreong, K.-N. Areerak, A. Srikaew, S. Sujitjorn, and P. Totarong, "System identification via adaptive Tabu search," in *Proc. IEEE Int. Conf. Ind. Technol. (ICIT)*, Aug. 2002, pp. 915–920.
[28] R. Phosung, K. Areerak, and K. Areerak, "Design and optimization of control system for more electric aircraft power systems using adaptive Tabu search algorithm based on state-variables-averaging model," *IEEE Access*, vol. 12, pp. 76579–76588, 2024.
[29] K-N. Areerak, T. Wu, S. V. Bozhko, G. M. Asher, and D. W. P. Thomas, "Aircraft power system stability study including effect of voltage control and actuators dynamic," *IEEE Trans. Aerosp. Electron. Syst.*, vol. 47, no. 4, pp. 2574–2589, Oct. 2011.
[30] A. Emadi, "Modeling of power electronic loads in AC distribution systems using the generalized state-space averaging method," *IEEE Trans. Ind. Electron.*, vol. 51, no. 5, pp. 992–1000, Oct. 2004.
[31] A. Emadi, "Modelling and analysis of multi-converter DC power electronic systems using the generalized state space averaging method," in *Proc. 27th Annu. Conf. IEEE Ind. Electron. Soc. (IECON)*, Dec. 2001, pp. 1001–1007.
[32] S.-B. Han, N.-S. Choi, C.-T. Rim, and G.-H. Cho, "Modeling and analysis of static and dynamic characteristics for buck-type three-phase PWM rectifier by circuit DQ transformation," *IEEE Trans. Power Electron.*, vol. 13, no. 2, pp. 323–336, Mar. 1998.
[33] T. Sopapirm, K.-N. Areerak, and K.-L. Areerak, "The mathematical model of a three-phase diode rectifier with multi-converter power electronic loads," in *Recent Researches in Power Systems and Systems Science*, 2011, pp. 100–105.
[34] C. Gao, "A cascade-formed accurate quasi-PR controller realization by pole-zero placement," *CPSS Trans. Power Electron. Appl.*, vol. 9, no. 1, pp. 51–62, Mar. 2024.
[35] W.-C. Chiang, "The application of a Tabu search metaheuristic to the assembly line balancing problem," *Ann. Operations Res.*, vol. 77, pp. 209–227, Jan. 1998.
[36] R. Ghiasi, M. R. Ghasemi, and M. Noori, "Comparative studies of metamodeling and AI-based techniques in damage detection of structures," *Adv. Eng. Softw.*, vol. 125, pp. 101–112, Nov. 2018.

JAKKRIT PAKDEETO received the B.Eng. (Hons.), M.Eng., and Ph.D. degrees in electrical engineering from the Suranaree University of Technology (SUT), Nakhon Ratchasima, Thailand, in 2013, 2015, and 2019, respectively. In 2019, he was a Researcher with the Institute of Research and Development, SUT. Since 2020, he has been a Lecturer with the Department of Teacher Training in Electrical Engineering, Faculty of Technical Education, King Mongkut's University of Technology North Bangkok (KMUTNB), Thailand. He has received the title of an Assistant Professor of electrical engineering, in 2021. His main research interests include stability analysis, power electronics, AI applications, control theory, and dc micro-grid systems.

ALISA THANOMMUANG was born in Nakhon Ratchasima, Thailand, in 1998. She received the B.Eng. (Hons.) and M.Eng. degrees in electrical engineering from the Suranaree University of Technology (SUT), Nakhon Ratchasima, in 2019 and 2022, respectively, where she is currently pursuing the Ph.D. degree in electrical engineering. Her main research interests include control theory, stability analysis, and instability mitigation in power systems.

KONGPOL AREERAK (Member, IEEE) received the B.Eng., M.Eng., and Ph.D. degrees in electrical engineering from the Suranaree University of Technology (SUT), Thailand, in 2000, 2003, and 2007, respectively. Since 2007, he has been a Lecturer and the Head of the Power Quality Research Unit (PQRU), School of Electrical Engineering, SUT. He received the title of an Associate Professor of electrical engineering, in 2015. His main research interests include active power filter, harmonic elimination, AI application, motor drive, and intelligence control systems.

KONGPAN AREERAK (Member, IEEE) received the B.Eng. and M.Eng. degrees in electrical engineering from the Suranaree University of Technology (SUT), Nakhon Ratchasima, Thailand, in 2000 and 2001, respectively, and the Ph.D. degree in electrical engineering from the University of Nottingham, Nottingham, U.K., in 2009. In 2002, he was a Lecturer with the Electrical and Electronic Department, Rangsit University, Thailand. Since 2003, he has been a Lecturer with the School of Electrical Engineering, SUT. He has received the title of an Associate Professor of electrical engineering, in 2015. His main research interests include system identifications, artificial intelligence applications, stability analysis of power systems with constant power loads, modeling and control of power electronic-based systems, and control theory.